

## 3D NUMERICAL SIMULATIONS OF LABORATORY MODELS OF ACCRETION SHOCKS IN YOUNG STELLAR OBJECTS

L. Ibgui<sup>1</sup>, I. Hubeny<sup>2</sup>, T. Lanz<sup>3</sup>, C. Stehlé<sup>1</sup>, M. González<sup>4</sup> and J.-P. Chièze<sup>4</sup>

**Abstract.** We show preliminary results of our numerical simulations of laboratory experiments of radiative shocks. Such experiments aim at understanding accretion shocks in young stellar objects. Three-dimensional non-stationary radiation hydrodynamics calculations were performed with the code HERACLES. X-UV spectra were then generated with the new three-dimensional radiative transfer code IRIS.

Keywords: Accretion, accretion disks, Radiative transfer, Hydrodynamics, Shock waves, Atomic processes

### 1 Introduction

Understanding the physics of radiative shocks in accretion columns is a prerequisite for a correct modeling of the accretion around young stellar objects. Now, it is possible to generate radiative shocks in laboratory. With such an asset, we can explore in detail various aspects of this physical phenomenon. We present a new generic 3D radiative transfer code, IRIS (Ibgui et al. 2012), that post-processes (radiation) (magneto) hydrodynamics (R)(M)HD simulations, in order to provide spectroscopic diagnostic information of a studied astrophysical object or structure, but also of laboratory generated structures. The main characteristics of IRIS are summarized in § 2. In § 3, we show a few preliminary results of our numerical simulations of experimentally generated radiative shocks. The RHD calculations are made with the well-tested code HERACLES (González et al. 2007).

### 2 IRIS: numerical schemes and capabilities of the code

IRIS is a new generic three-dimensional spectral radiative transfer code (Ibgui et al. 2011, 2012), which generates synthetic spectra or images, by post-processing snapshots provided by 3D (R)(M)HD simulations. IRIS solves the static 3D monochromatic radiative transfer equation (RTE) in the observer's frame, and in a nonuniform Cartesian grid. For any snapshot identified by instant  $t$ , the code determines the specific intensity  $I(\mathbf{r}, \mathbf{n}, \nu, t)$  for any specified position  $\mathbf{r}$ , photon direction  $\mathbf{n}$ , and frequency  $\nu$ . The current version of the code assumes local thermodynamic equilibrium (LTE).

The solver employs the short-characteristics method (Mihalas et al. 1978; Olson & Kunasz 1987; Kunasz & Auer 1988; Kunasz & Olson 1988). The RTE is solved in its integral form that is discretized along each short-characteristic. The physical quantities at the intersections of the short-characteristic with the faces of the grid cells are determined by piecewise cubic locally monotonic interpolations. The variations of these quantities along a short-characteristic are approximated by the same type of interpolants. The interpolation scheme consists of a cubic Hermite polynomial combined with weighted harmonic mean node derivatives (Brodie 1980; Fritsch & Butland 1984; Auer 2003).

IRIS can handle the effects of the macroscopic (non-relativistic) velocities: where necessary, the code subdivides a short-characteristic, in order to correctly deal with the Doppler shift of photon frequency due to velocity

<sup>1</sup> LERMA, Observatoire de Paris, CNRS, UMPC, 5, place J. Janssen, 92195 Meudon Cedex, France

<sup>2</sup> Department of Astronomy, Steward Observatory, The University of Arizona, 933 N. Cherry Ave, Tucson, AZ 85721-0065, USA

<sup>3</sup> Laboratoire J.-L. Lagrange, Université de Nice Sophia Antipolis, CNRS, Observatoire de la Côte d'Azur, Boulevard de l'Observatoire, B.P. 4229, 06304 Nice Cedex 4, France

<sup>4</sup> AIM, CEA/DSM/IRFU, Université Paris Diderot, 91191 Gif-sur-Yvette, France

gradient between two positions. The code also computes the monochromatic radiation moments (mean intensity, radiation flux vector, and radiation pressure tensor), by angular integration of the specific intensity. IRIS can deal with periodic boundary conditions in the case of a medium with an infinite extension in its horizontal plane, such as a stellar atmosphere or an accretion disk. For detailed explanations of all the related algorithms, we refer the reader to the paper by Ibgui et al. (2012).

### 3 3D numerical simulations of laboratory shocks: preliminary results

#### 3.1 Brief description of the experimental case

Radiative shocks, i.e., shocks that are structured by radiation within a plasma, appear in accretion columns around young stellar objects, and have a strong contribution to the spectral signature of these objects. This is why it is important to have a good understanding of the physics of these shocks. Now, it is possible to perform laboratory experiments that simulate radiative shocks. Laser driven shocks were recently produced in the PALS (Prague Asterix Laser System) facility in Prague (Bouquet et al. 2004; Reighard et al. 2006; Stehlé et al. 2010, 2012). The experimental target consists of a 6 mm long shock-tube with a uniform  $0.4 \times 0.4 \text{ mm}^2$  section. The tube is full of pure xenon, initially at room temperature, under pressure of typically 0.2 to 0.3 bar (order of magnitude of the density:  $10^{-3} \text{ g cm}^{-3}$ ). The laser hits a piston at the base of the tube. The resulting motion of the piston (at constant velocity of  $60 \text{ km s}^{-1}$  relative to the laboratory frame) generates a non-stationary flow with a radiative shock. For further details, the reader is referred to the above papers. We have simulated the flow in the shock-tube, along with the spectra emitted by the flow, as presented in § 3.2 and § 3.3 below.

#### 3.2 Radiation hydrodynamics simulation with HERACLES

HERACLES is a three-dimensional radiation hydrodynamics code whose radiative equations, described by the  $M_1$  model (Levermore 1996; Dubroca & Feugeas 1999), are solved with a second-order Godunov type algorithm (González et al. 2007). The influence of the radiation on the shock structure was demonstrated by previous two-dimensional simulations with HERACLES (González et al. 2009).

For the present study, three-dimensional simulations of the flow in the shock-tube were performed. In Fig. 1, left panel, the piston is represented by the hatched face, and the shock propagates in positive  $z$ -direction. The lateral walls and the base on the right have a zero albedo, which means that there is no wall reflexion: the photons can freely escape. In addition, there is no photon incoming from the outside through these five faces. As for the base on the left, i.e., the piston, we assume that it radiates like a black body at the local temperature of the plasma.

HERACLES uses a perfect gas equation of state that includes the mean ionization stage of the plasma. The code uses grey opacities (Mirone et al. 1997). We present here some preliminary results. Fig. 2, left panel, displays the variation of the density and the temperature along the central axis of the shock-tube, for a snapshot defined at time  $t = 4 \text{ ns}$  after the piston launch. Along axis, the distance between the shock front and the piston is  $z_{\text{shock}} = 0.019 \text{ mm}$ . The gas is heated upstream (large  $z$  values) by the photons generated by the shock: this part of the flow is the radiative precursor (Mihalas & Mihalas 1984). Fig. 2, right panel, displays a map of the temperature distribution over a cross-section ( $x, y$ ) of the shock-tube, in the precursor at  $z = 0.066 \text{ mm}$ . This figure shows evidence of the three-dimensional nature of the flow. Detailed descriptions of the results will be provided in a future paper (Ibgui et al. 2012, in preparation).

#### 3.3 X-UV Spectra obtained with IRIS: some early results

With IRIS, we post-processed the results provided by HERACLES. We used xenon monochromatic opacities calculated by the Screened Hydrogenic Model (Eidmann 1994; Michaut et al. 2004). They include bound-bound, bound-free, and free-free processes. Fig. 1, left panel, defines our notations.  $(O, x, y, z)$  is a coordinate system that is linked to the piston's frame. The position of a given point  $M$  in the flow is identified by its coordinates  $(x, y, z)$ . The direction of propagation of the radiation,  $\mathbf{n}$ , is defined with respect to the basis  $(\mathbf{e}_x, \mathbf{e}_y, \mathbf{e}_z)$ , by the polar angle  $\theta$  between  $\mathbf{n}$  and  $\mathbf{e}_z$ , and by the azimuthal angle  $\varphi$ , between  $\mathbf{e}_x$  and the projection of  $\mathbf{n}$  on the  $x - y$  plane. To be consistent with the radiation boundary conditions adopted by HERACLES (see Section 3.2), we assume a null incoming specific intensity from the lateral walls and from the base on the right. In addition, the incoming specific intensity from the piston (base on the left) equals the Planck function at the local temperature of the plasma. Finally, there is no wall reflexion, so that the photons can freely escape.

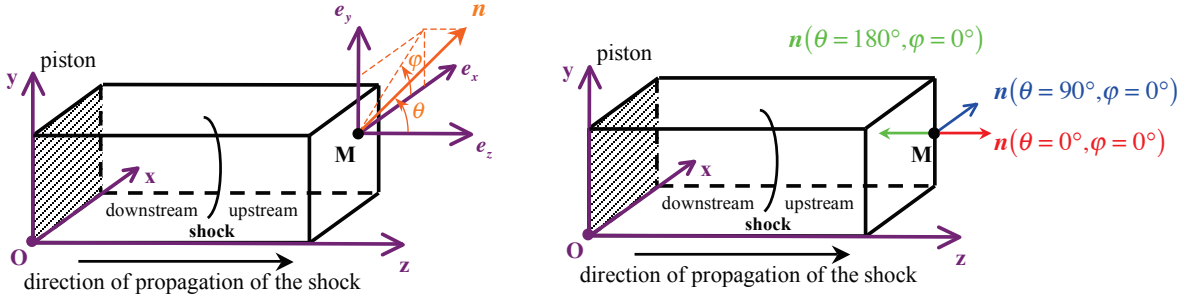


**Fig. 1.** Xenon filled tube, in which the radiative shock is generated by the motion of the piston in positive  $z$ -direction. **Left:** position of a given point  $M$  and a direction  $\mathbf{n}$  of propagation of the radiation. **Right:** position  $M$  and three directions for which we show spectra in § 3.3.

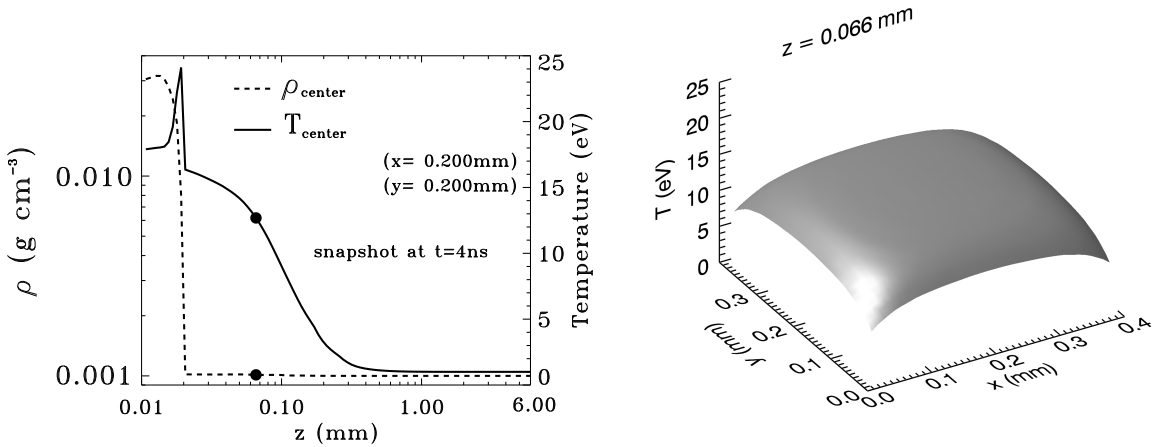


**Fig. 2. Left:** Density ( $\text{g cm}^{-3}$ ) and temperature (eV, where 1 eV corresponds approximately to 11604.5 K) at the center of the shock-tube versus distance  $z$  from the piston, at a given instant  $t = 4$  ns. **Right:** Temperature distribution over the  $(x, y)$  cross-section at position  $z = 0.066$  mm that is represented by the thick dots in the left panel.

Fig. 3 shows X-UV spectra of specific intensities that emerge from the flow at point  $M$  in the border (lateral) face defined by  $x = 0.40$  mm,  $y = 0.20$  mm, and  $z = 0.011$  mm. The curves in the figure represent the specific intensities in three directions defined by  $\varphi = 0^\circ$ , and,  $\theta = 0^\circ$  (red),  $\theta = 90^\circ$  (blue), and  $\theta = 180^\circ$  (green). Fig. 1, right panel, clarifies the position of  $M$  and the directions of the radiation. The temperature profile along  $z$ -axis to which  $M$  belongs is depicted by the solid line in the right panel of Fig. 3. Note that the temperature profile differs for each different  $z$ -axis. For comparison, we plot with a dashed line the profile for the central  $z$ -axis. The peak of the temperature, which corresponds to the position of the shock, is, for the central profile, ahead of the peak for the border profile. This is consistent with the curved shape of the temperature map shown in Fig. 2, right panel.  $M$  is in the shocked part of the flow.

The spectra clearly show the anisotropy of the radiation downstream of the shock. The specific intensity  $I_\nu(\theta = 0^\circ)$  fits the Planck function at the local temperature of the plasma. This value of the intensity is mainly due to the emission from the piston. The specific intensity in the perpendicular direction  $I_\nu(\theta = 90^\circ)$  is close to the Planck function, but we see emission and absorption lines contributions. The specific intensity in the opposite direction  $I_\nu(\theta = 180^\circ)$  is very different from the two preceding ones. Since there is no photon incoming from the base on the right of the tube, the emission here is mainly due to the photon emitted in the shock and, to a lesser extent, to the photons emitted in the precursor region. For the three directions, the emission in the X-rays ( $\lambda \leq 10$  nm,  $h\nu \geq 124$  eV) is weaker than the emission in the UV domain. For  $I_\nu(\theta = 180^\circ)$ , the largest emission peaks are between 55 eV (22.5 nm) and 115 eV (10.8 nm). In a future paper (Ibgui et al. 2012, in preparation), we will present results for more positions, specifically around the shock and in the precursor.

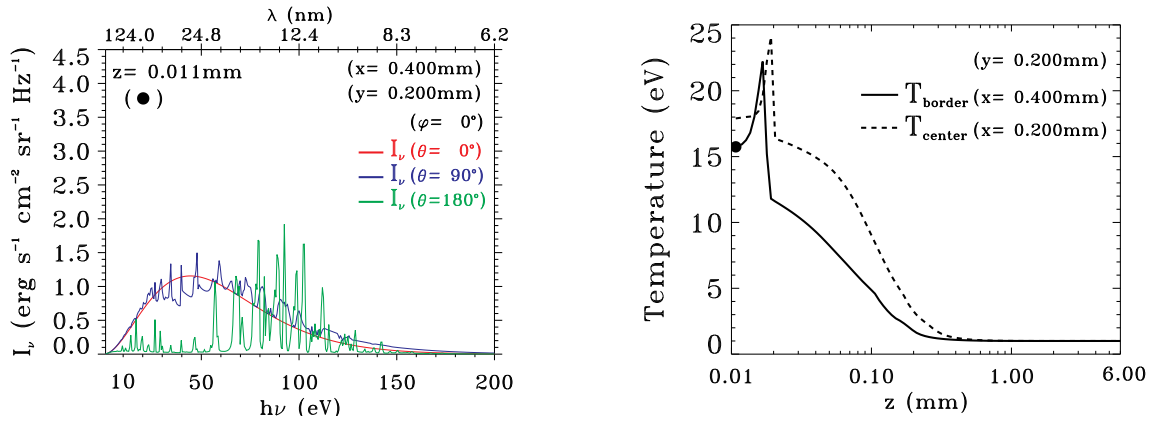


**Fig. 3.** **Left:** spectral specific intensities emerging from the shock tube at  $(x, y, z) = (0.400, 0.200, 0.011)$  mm. Intensities in three directions are represented:  $\varphi = 0^\circ$ , and  $\theta = 0^\circ$  (red),  $\theta = 90^\circ$  (blue), and  $\theta = 180^\circ$  (green). **Right:** temperature profiles along two  $z$ -axes: a border axis  $x = 0.400$  mm, the central axis  $x = 0.200$  mm. For both,  $y = 0.200$  mm.  $z = 0.011$  mm position is represented by a thick dot in the profile. See § 3.3 for explanations.

#### 4 Conclusion

Preliminary results of three-dimensional non-stationary radiation hydrodynamics simulations with HERACLES, along with spectra simulated by IRIS prove the three-dimensional nature of a radiative shock, the anisotropy of the radiation, and the strong dependence of the radiation with the frequency. Further results will be detailed in a paper, Ibgui et al. (2012), in preparation.

The work is supported by French ANR, under grant 08-BLAN-0263-07. IH acknowledges the travel support from the Observatoire de Paris.

#### References

- Auer, L. 2003, in Astronomical Society of the Pacific Conference Series, Vol. 288, Stellar Atmosphere Modeling, ed. I. Hubeny, D. Mihalas, & K. Werner, 3
- Bouquet, S., Stéhlé, C., Koenig, M., et al. 2004, Physical Review Letters, 92, 225001
- Brodie, K. W. 1980, in Mathematical Methods in Computer Graphics and Design, K. W. Brodie ed., Academic Press, London, 1
- Dubroca, B. & Feugeas, J. 1999, Academie des Sciences Paris Comptes Rendus Serie Sciences Mathematiques, 329, 915
- Eidmann, K. 1994, Laser and Particle Beams, 12, 223
- Fritsch, F. N. & Butland, J. 1984, SIAM J. Sci. Stat. Comput., 5, 300
- González, M., Audit, E., & Huynh, P. 2007, A&A, 464, 429
- González, M., Audit, E., & Stehlé, C. 2009, A&A, 497, 27
- Ibgui, L., Hubeny, I., Lanz, T., & Stehlé, C. 2011, in SF2A-2011: Proceedings of the Annual meeting of the French Society of Astronomy and Astrophysics, ed. G. Alecian, K. Belkacem, R. Samadi, & D. Valls-Gabaud, 485–489
- Ibgui, L., Hubeny, I., Lanz, T., & Stehlé, C. 2012, submitted to A&A
- Kunasz, P. & Auer, L. H. 1988, J. Quant. Spec. Radiat. Transf., 39, 67
- Kunasz, P. B. & Olson, G. L. 1988, J. Quant. Spec. Radiat. Transf., 39, 1
- Levermore, C. D. 1996, Journal of Statistical Physics, 83, 1021
- Michaut, C., Stehlé, C., Leygnac, S., Lanz, T., & Boireau, L. 2004, European Physical Journal D, 28, 381
- Mihalas, D., Auer, L. H., & Mihalas, B. R. 1978, ApJ, 220, 1001
- Mihalas, D. & Mihalas, B. W. 1984, Foundations of radiation hydrodynamics
- Mirone, A., Gauthier, J. C., Gilleron, F., & Chenais-Popovics, C. 1997, J. Quant. Spec. Radiat. Transf., 58, 791
- Olson, G. L. & Kunasz, P. B. 1987, J. Quant. Spec. Radiat. Transf., 38, 325
- Reighard, A. B., Drake, R. P., Dannenberg, K. K., et al. 2006, Physics of Plasmas, 13, 082901
- Stehlé, C., González, M., Kozlova, M., et al. 2010, Laser and Particle Beams, 28, 253
- Stehlé, C., Kozlová, M., Larour, J., et al. 2012, Optics Communications, 285, 64